that his effective mass was measured at a Fermi energy up to 0.05 eV above the bottom of the conduction band. The donor binding energy calculated from the effective-mass approximation using a mass of $0.19m_e$ is approximately 30% smaller than the experimentally determined binding energy obtained on the assumption that the $n=2$ excited state is effective-mass-like. For the $n=2$ states, the effective-mass approximation should be good. For the $n=1$ state, it is evident that central-cell corrections become important.

There is still some uncertainty as to the dielectric constants in ZnO. This will have the greatest effect on the binding-energy determination. It will also have a small effect on the effective-mass value.

PHYSICAL REVIEW VOLUME 185, NUMBER 3 15 SEPTEMBER 1969

Piezoreflectance of Germanium from 1.9 to 2.8 eV

D. D. SELL AND E. O. KANE
Bell Telephone Laboratories, Murray Hill, New Jersey 07974
(Received 28 February, 1969)

The dependence of the imaginary part of the dielectric function, $\epsilon_2(\omega)$, on a small-amplitude ac stress in the energy range from 1.9 to 2.8 eV for germanium is analyzed. The dependence of the differential $\delta\epsilon_2$ on polarization and stress direction is described in terms of three symmetry-adapted response functions: $W_1(\omega)$, $W_3(\omega)$, and $W_5(\omega)$. The function $W_1(\omega)$ characterizes the response to hydrostatic stress. [001] uniaxial stress generates $W_1(\omega)$ and $W_3(\omega)$ while [111] stress generates $W_1(\omega)$ and $W_5(\omega)$. The $W_j(\omega)$ contain contributions $W_j^{\text{shift}}(\omega)$ from energy-band shifts, and also $W_j^{\text{mvar}}(\omega)$ due to optical-matrix-element variation. We find $W_3^{\text{shift}}(\omega)=0$, which implies that the critical points near 2.1 and 2.3 eV lie in the [111] direction (Λ) or at the L point, in agreement with previous work. $W_1(\omega)$ contains almost purely energy-shift effects, which leads to the derivative of the unstrained $\epsilon_2(\omega)$ function, since hydrostatic shifts lead to very little wave-function mixing. $W_1(\omega)$ and $W_3(\omega)$ give very distinct line shapes which are characteristic of energy-band shifts and matrix-element variation, respectively. Here $W_5(\omega)$ can be represented as a linear combination of $W_1(\omega)$ and $W_3(\omega)$. We can account for the observed line shapes quantitatively on the assumption that $\epsilon_2(\omega)$ consists of two distinct contributions $\epsilon_2^+(\omega)$ and $\epsilon_2^-(\omega)$ from each spin-orbit-split band, which are identical except for an energy shift equal to the spin-orbit splitting. This analysis yields four deformation potential constants: D_1^1, D_1^5, D_3^3 and D_3^5. The quantities D_1^1 and D_1^5 agree with previous measurements by Zallen and Paul and by Gerhardt. D_3^3 agrees with the value determined by Pollak and Cardona using a dc stress method, while D_3^5 differs by a factor of 4. The origin of this discrepancy is not presently understood, but recent calculations by Saravia and Brust tend to support this value.

I. INTRODUCTION AND CONCLUSIONS

THE pioneering work of Seraphin[1] initiated a great deal of study of optical critical-point structure by differential methods, chiefly piezoreflectance[2,3] and electroreflectance.[4] One of the advantages of these methods is the increase in sensitivity over dc measurements. Another advantage is the information about critical point symmetry which can be inferred from the symmetry-breaking property of differential perturbations. This latter advantage has not been as widely exploited because the difficulties of measurement and interpretation are somewhat greater.

In this paper, we use polarized light to study the structure in the reflectivity of germanium (Ge) in the region from 1.9 to 2.8 eV, using an ac piezoreflectance technique. While measurements of this type on Ge have not yet been reported, they are very closely related to measurements made under high dc strain reported by Gerhardt[5] and by Pollak and Cardona.[6] We feel the ac stress method is somewhat simpler. It can also be applied to materials which cannot sustain strains high enough to produce observable splittings of critical point structure.

It is generally accepted that the structure between 2.1 and 2.3 eV in Ge results from critical points in the Λ-direction, or at the L point with transitions occurring between an $L_{3'}$ (Λ_3) valence band and an L_1 (Λ_1) conduction band. The $L_{3'}$ (Λ_3) double degeneracy is lifted by spin-orbit interaction of $\sim$0.2 eV. Most band calculations find an M_0 singularity at the L point and an M_1 singularity along the Λ direction.[7] The two singularities are within a few tenths of an eV of each other. The strong structure at 2.1 and 2.3 eV is generally

[1] B. O. Seraphin and R. B. Hess, Phys. Rev. Letters **14**, 138 (1965); B. O. Seraphin and N. Botta, Phys. Rev. **139**, A560 (1965); **140**, A1716 (1965); **145**, 628 (1966).
[2] W. E. Engeler, M. Garfinkel, J. J. Tiemann, and H. Fritzsche, Phys. Rev. Letters **14**, 1069 (1965); G. W. Gobeli and E. O. Kane, *ibid.* **15**, 142 (1965); U. Gerhardt, D. Beaglehole, and R. Sandrock, *ibid.* **19**, 309 (1967).
[3] M. Garfinkel, J. J. Tiemann, and W. E. Engeler, Phys. Rev. **148**, 695 (1966).
[4] M. Cardona, K. L. Shaklee, and F. H. Pollak, Phys. Rev. **154**, 696 (1967).
[5] U. Gerhardt, Phys. Rev. Letters **15**, 401 (1965); Phys. Status Solidi **11**, 801 (1965).
[6] F. H. Pollak and M. Cardona, Phys. Rev. **172**, 816 (1968).
[7] D. Brust, Phys. Rev. **134**, A1337 (1964); L. R. Saravia and D. Brust, *ibid.* **176**, 915 (1968).

TABLE I. Symmetry conditions on the component of W_j due to energy-band shifts. From Ref. 15.

Critical point location	Symmetry condition for nondegenerate bands
$\mathbf{k}=0$	$W_3^{\text{shift}}=W_5^{\text{shift}}=0$
$\mathbf{k}=\Delta$	$W_5^{\text{shift}}=0$
$\mathbf{k}=\Lambda$, L	$W_3^{\text{shift}}=0$
$\mathbf{k}=\Sigma$, U_2 symmetry	$W_5^{\text{shift}}=0$

identified as coming from the spin-orbit-split M_1 singularity along the Λ direction.[8]

L-point transitions have been identified by Potter[9] as occurring at 1.74 and 1.94 eV at room temperature. The structure is very weak and we feel the interpretation is insecure. Ghosh[10] has used electroreflectance measurements to identify L-point transitions at 2.05 and 2.24 eV at room temperature. This structure strongly overlaps the Λ-point structure, and we feel that the problem of electroreflectance line shapes is not sufficiently well in hand to permit such interpretations to be made with confidence. However, our conclusions are not in conflict with his interpretation.

Coulomb effects at M_0[11] and M_1[12,13] singularities have been studied in the effective mass approximation. The line-shape modifications are very strong. The effective-mass approximation is probably not adequate to study critical points whose energy separation is only a few tenths of an eV. It is not even clear to what extent structure due to Coulomb effects could be assigned to the singularities separately.

For small lifetime broadening, excitonic effects at an M_0 singularity are unambiguously characterized by sharp peak structure in ϵ_2. For heavy lifetime broadening the spectrum resembles a square edge which has been folded with a Lorentzian. The relatively abrupt rise on the low-energy side of the critical point is the main distinguishing feature. For an M_1 singularity,[13] the strongest structure results from the lowest two-dimensional bound state of the light mass degrees of freedom. This structure is characterized by an asymmetric peak whose steepest slope is on the high-energy side, just the opposite of the M_0 case. The line shapes we obtain are characterized by steep slopes on both high- and low-energy sides, and it is tempting to suggest that this results from the combination of an M_0 and M_1 singularity separated in energy by about 0.1 to 0.2 eV. The energy scale for Coulomb effects is determined by the two-dimensional light-mass binding energy,[13] which is only 0.01 eV for Ge. This is small compared to the lifetime broadening energy, but not so small that Coulomb effects can be safely ignored. Saravia and Brust[14] have found agreement with piezoreflectance line shapes on a pure density-of-states basis. Possibly a combination of band structure and Coulomb effects are involved, with neither being dominant.

The most general linear relation between the dielectric constant and the strain in a cubic crystal can be described in terms of the three functions $W_1(\omega)$, $W_3(\omega)$, and $W_5(\omega)$.[15] The function W_1 is the normalized response to hydrostatic stress, while W_3 and W_5 describe the polarization dependence induced by [001] and [111] uniaxial stresses, respectively. Contributions to these functions are of two types W_j^{shift} caused by energy band shifts, and W_j^{mvar} due to matrix element variation induced by strain. W_j^{shift} is a simple indicator of critical-point symmetry for nondegenerate bands as shown in Table I.

For the 2.1- and 2.3-eV structure in Ge, we find $W_3^{\text{shift}}=0$, which indicates a critical point at L or in the Λ-direction. This conclusion agrees with band-structure calculations, and also with Gerhardt[5] and Pollak and Cardona's[6] conclusions based on the effect of large dc strains.

W_1^{mvar} is expected to be very small, because hydrostatic strain mixes only bands of the same symmetry which are separated by several eV, or more, at the same point in k space. Then if the hydrostatic deformation potential D_1^1 does not vary appreciably over the region of k space contributing to $\epsilon_2(\omega)$, we expect that $W_1(\omega)\sim d\epsilon_2/d\omega$. We have tested this conclusion using our determination of W_1 and Potter's measurement of ϵ_2,[9] and find it to be well obeyed.

The measured values of W_1 and W_3, then, give a very clean separation of the effects W^{shift} and W^{mvar}, and we find two very distinct and characteristic line shapes associated with $W_1=W^{\text{shift}}$ and $W_3=W^{\text{mvar}}$. The function W_5 is expected to include both effects, and we find that it can be represented quite well by a linear combination of W_1 and W_3.

We can analyze our data more quantitatively if we make several assumptions which are suggested by the effective mass (2 band) approximation. Specifically, we assume that we have two energy bands $\pm$ identical except for the spin-orbit splitting, which give contributions $\epsilon_2^{\pm}(\omega)$ to the dielectric function. These functions are simply shifted relative to each other by 2λ, the spin-orbit splitting, i.e., $\epsilon_2^{+}(\omega+2\lambda)=\epsilon_2^{-}(\omega)$. These functions are experimentally determined and hence may be assumed to include Coulomb effects.

We assume that the effect of strain on these bands can be described by four deformation-potential constants D_1^1, D_1^5, D_3^3, and D_3^5.[15] The constant D_1^1 represents hydrostatic strain, where all bands are shifted by the same energy. Here D_1^5 represents a shift of both bands at a given critical point $\mathbf{k}_0$ by the same

[8] J. C. Phillips, Phys. Rev. **133**, A452 (1964).
[9] R. F. Potter, Phys. Rev. **150**, 562 (1966).
[10] A. K. Ghosh, Phys. Rev. **165**, 888 (1968).
[11] R. J. Elliott, Phys. Rev. **108**, 1384 (1957).
[12] B. Velický and J. Sak, Phys. Status Solidi **16**, 147 (1966); J. Hermanson, Phys. Rev. **166**, 893 (1968).
[13] E. O. Kane Phys. Rev. **180**, 852 (1969).
[14] L. R. Saravia and D. Brust, Phys. Rev. **178**, 1240 1969.
[15] E. O. Kane, Phys. Rev. **178**, 1368 (1969). This paper provides the ground work for the symmetry results presented here. Our notation for the deformation potentials is nonstandard. We prefer it because it is "universal" for all symmetry situations.

amount but a different shift for equivalent $\mathbf{k}_0$. Finally, D_3^3 and D_3^5 do not lead to band shifts (up to terms linear in the strain), but do lead to wave-function admixture and changes in optical matrix elements which are linear in the strain. In Sec. IV, we discuss the relation between our deformation potential constants and the standard definitions.

The above assumptions can be justified on the basis of an effective mass (2 band) approximation when the kinetic energy (or exciton binding energy) relative to the band edge is small relative to the spin-orbit splitting. This assumption may be accurate for the peaks at 2.1 and 2.3 eV, but less accurate for energies $\gtrsim 0.2$ eV away from the peaks. If a large region of k space does, in fact, contribute to the peaks, then our assumptions would require that none of our D_j^i vary strongly over that region.

On the basis of the above assumptions, we are able to give a reasonably self-consistent quantitative analysis of our data. We can decompose ϵ_2 into the two contributions $\epsilon_2^{\pm}$ and show that $W_3 \sim \epsilon_2^+ - \epsilon_2^-$. We also obtain values for the four deformation potentials D_1^1, D_1^5, D_3^3, and D_3^5. The energy-shift parameters D_1^1 and D_1^5 agree with earlier high stress measurements by Zallen and Paul[16] and by Gerhardt.[5] D_3^3 and D_3^5 are determined from matrix element variation. The influence of matrix element variation was noted both by Gerhardt[5] and by Pollak and Cardona.[6] Pollak and Cardona's discussion of the effect is very similar to ours, although our treatment is somewhat more general.

Pollak and Cardona[6] have determined D_3^3 and D_3^5 using a dc stress analysis. They find agreement with the corresponding parameters measured at $k=0$. We agree with Pollak and Cardona for D_3^3 but our value for D_3^5 is smaller by a factor of 4. The source of this discrepancy is not presently understood, but recent calculations by Saravia and Brust[14] tend to support our value.

In summary, we have measured the three fundamental linear dielectric-stress functions W_1, W_3, and W_5 for Ge from 1.9 to 2.8 eV. We have found that W_1 represents energy-shift effects, W_3 represents optical matrix element variation, and W_5 is a linear combination of the two. The fact that $W_3^{\text{shift}}=0$ implies that the critical point is at Λ or L. From line-shape studies, we suggest that the structure may involve Coulomb effects at an M_0 and M_1 singularity separated by ~ 0.1 to 0.2 eV, although band structure effects appear to be important also, as shown by Saravia and Brust.[14] We have determined the four deformation potential parameters D_1^1, D_1^5, D_3^3, and D_3^5 for the critical point to a reproducibility of the order of 10%. The accuracy depends on the correctness of the interpretation. We feel that D_3^3 is the least certain $(+1,-0.5$ eV). The ratio D_3^5/D_3^3 is measured more accurately, but D_3^5 is limited by the accuracy of D_3^3. Our results indicate that the present technique should be applicable to a large number of materials with nondegenerate critical points, and should be easier to apply than the dc strain method.

[16] R. Zallen and W. Paul, Phys. Rev. 155, 703 (1967).

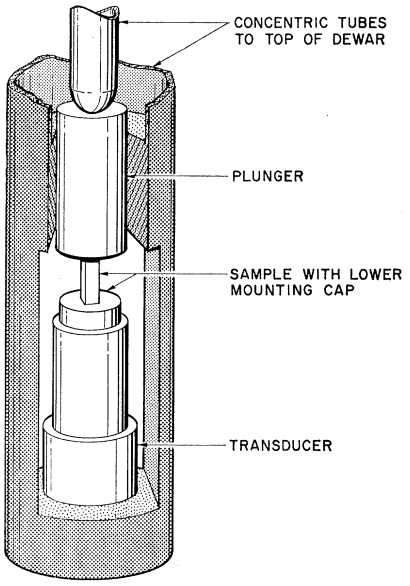

FIG. 1. Schematic representation of the sample press. This unit is mounted on the cold finger of a helium cryostat.

II. EXPERIMENTAL DETAILS

Samples of intrinsic, single-crystal Ge were oriented to within 0.5 deg by x-ray diffraction and cut into 1 mm×1 mm×10 mm rectangular parallelepipeds such that the long axis was either a ⟨001⟩ or a ⟨111⟩ direction. One sample face was carefully polished to remove surface damage and to obtain a good optical finish before one end was epoxied into a stainless steel end cap.[17] The samples were given a final cleaning in hydrofluoric acid before they were mounted in the stress apparatus.

The samples were mounted in vacuum on a cold finger in a helium cryostat. A diagram of the sample press is shown in Fig. 1. A dc and superimposed ac pneumatic force was applied to a piston at the top of the Dewar and was transmitted to the sample through two concentric stainless-steel tubes.

In an early version of the apparatus a modified commercial rotary value was driven with a dc motor so that it alternately filled and exhausted the pneumatic chamber and thereby modulated the force on the piston.[18] This valve, which proved to have a short lifetime, was later replaced with a high-speed solenoid valve.

[17] Various samples were mechanically polished and etched with CP-4, electropolished, and syton polished. (Syton is produced by Monsanto Chemical Co.) No differences were observed except that the syton polished samples which had the best optical finish tended to give the smallest offsets.

[18] A. J. Williams (unpublished).

The force on the sample was monitored with a Kistler 912 quartz force transducer in contact with the sample within the Dewar. The transducer output was amplified with a Kistler 503 charge amplifier and the fundamental frequency component of the force was monitored with a PAR 121 detector used as an ac voltmeter.

In typical operation, an ac force of 5 kg rms at 90 Hz was superimposed on a dc level of comparable magnitude. For such forces (strains of approximately 2×10^{-4}), the $\delta R/R$ signal was proportional to the ac force and no dependence on the dc stress level was detected.

To our knowledge this is the first report of such a stress modulator for piezo-optic experiments. We believe it offers characteristics not easily realized with other stress modulation apparatus. These characteristics include: (1) Relatively large stresses (at least a factor of 5 larger than those used here) can be applied to samples at low temperatures without the complications of resonant operation. (2) The dc and ac stress components can be monitored during the experiment to an accuracy of at least 5%. (3) The operation of the modulation apparatus is very independent of sample characteristics.

Light from a 150-W quartz iodide lamp (or tungsten ribbon lamp) was passed through a 0.3-m Mcpherson 218 monochromator, plane polarized by a Glan-Thompson polarizer at the exit slit, focused onto the sample at approximately 7 deg from normal incidence, and was detected by an EMI 9558 photomultiplier. The instrumental resolution was better than 0.01 eV.

The ratio $\delta R/R$ was measured in the conventional manner by varying the photomultiplier gain (by electronically varying its high voltage) such that the dc signal, which is proportional to R, was held constant at 1.0 V. The ac signal at the stress modulation frequency, which is then a direct measure of $\delta R/R$, was phase sensitively detected with a PAR HR-8. Digital electronics was used to record the signal on punched paper tape for later computer analysis.

In early experiments we had considerable difficulty reproducing the amplitudes of the $\delta R/R$ data and also observed small variations in the shapes of the traces. It was found that this was caused by bending of the sample. The problem is that the surface stress, which determines the optical signal, differs from the average stress measured by the transducer. For a bar which is both bent and compressed the surface stress can be either larger or smaller than the average stress (and can also have nonuniaxial character).

It was found that careful alignment alleviated this difficulty. The stress apparatus, especially the sample mount shown in Fig. 1, was accurately machined to minimize the possibility of applying a bending moment to the sample. The ends of the sample were lapped flat and perpendicular to the sample axis. Care was also taken to mount the sample in its end cap such that the sample and plunger axes were parallel. Finally, a three-mil thick soft copper foil was placed between the plunger and the top of the sample to further reduce the effects of imperfect alignment. With such precautions, the amplitude of the $\delta R/R$ data for different samples could be reproduced to within 10%.

A common difficulty in optical modulation experiments (especially piezo-modulation) is that there is a spurious, energy-independent variation of the zero level of the $\delta R/R$ data. This so called offset can arise from vibration induced in the apparatus. For our apparatus (when properly aligned) nearly all the offset arises from the relative motion of the optical beam and the sample surface. For a smooth surface without pits or scratches, the offset is insignificantly small. Since it is difficult to experimentally measure the offset, an analytic procedure discussed in Sec. IV was used to determine it. The data presented here have been corrected for offset.

The accuracy to which we can determine the deformation potential constants depends upon factors such as: (1) signal to noise reproducibility of the data, (2) systematic error in calibration of the apparatus, and (3) uncertainties of the data analysis. We estimate that the first two sources introduce less than a $\pm10\%$ error. The third item will be discussed further in Sec. IV.

III. THEORETICAL BACKGROUND

The quantity ϵ_2 the absorptive or imaginary part of the dielectric function, is the most important property to study from a theoretical point of view. It can be deduced from the measured reflectivity using the Kramers-Kronig relations.[19] For the case of differential perturbations, the appropriate formulas have been given by Garfinkel, Tiemann, and Engeler.[3] One first computes the auxiliary quantity, $\delta\theta$ by

$$\delta\theta(\omega_0)=\frac{1}{2\pi}\int_0^\infty \frac{d}{d\omega}\left(\frac{\delta R}{R}\right)\ln\left|\frac{\omega+\omega_0}{\omega-\omega_0}\right|d\omega. \tag{3.1}$$

The change $\delta\epsilon_2$ is then given by

$$\delta\epsilon_2=B\tfrac{1}{2}(\delta R/R)-A\delta\theta, \tag{3.2}$$

$$A\equiv n(\epsilon_1-1)-k\epsilon_2, \tag{3.3}$$

$$B\equiv k(\epsilon_1-1)+n\epsilon_2,$$

$$(n+ik)^2=\epsilon_1+i\epsilon_2.$$

The quantities entering into Eq. (3.3) refer to the unstrained crystal, which we take from Potter's measurements.[9]

The actual limits of integration used were 1.9 to 2.8 eV. Although this range is much smaller than is customary in dc reflectivity measurements, we are partially justified in our choice because $\delta R/R$ is dominated by the region of interest to a much greater extent than is R itself. The main effect of extending the limits

[19] F. C. Jahoda, Phys. Rev. **107**, 1261 (1957); H. R. Philipp and E. A. Taft, *ibid.* **113**, 1002 (1959).

of integration would probably be to change the average value of $\delta\epsilon_2$, a quantity which is not very important to our analysis.

The analysis of the linear strain dependence $\epsilon_2(\omega)$ is most simply described in terms of the three functions $W_1(\omega)$, $W_3(\omega)$, and $W_5(\omega)$ which relate the components of the change in the dielectric tensor $\boldsymbol{\epsilon}_2$ to the strain tensor $\mathbf{e}$ in a symmetry adapted basis.[15]

$$\begin{aligned}&\delta\epsilon_{2,1}=W_1e_1,\\&\delta\epsilon_{2,3\gamma}=W_3e_{3\gamma};\quad\gamma=\alpha,\beta,\\&\delta\epsilon_{2,5\gamma}=W_5e_{5\gamma};\quad\gamma=xy,\,xz,\,yz.\end{aligned}\tag{3.4}$$

The irreducibly transforming components of any second-rank symmetric tensor may be written

$$\begin{aligned}&e_1\equiv(e_{xx}+e_{yy}+e_{zz})/\sqrt{3},\\&e_{3\alpha}\equiv(2e_{zz}-e_{xx}-e_{yy})/\sqrt{6},\\&e_{3\beta}\equiv(e_{xx}-e_{yy})/\sqrt{2},\\&e_{5xy}\equiv e_{xy},e_{5xz}\equiv e_{xz},e_{5yz}\equiv e_{yz}.\end{aligned}\tag{3.5}$$

The definition of $\epsilon_{2,j\gamma}$ is completely analogous.

The three W functions are most conveniently determined by applying uniaxial stress in the [001] and [111] directions which generates the strain components:

[001] stress

$$e_1=(s_{11}+2s_{12})T/\sqrt{3},\tag{3.6}$$

$$e_{3\alpha}=(\sqrt{\tfrac{2}{3}})(s_{11}-s_{12})T,\tag{3.7}$$

[111] stress

$$e_1=(s_{11}+2s_{12})T/\sqrt{3},\tag{3.8}$$

$$e_{5xy}=e_{5xz}=e_{5yz}=s_{44}T/6.\tag{3.9}$$

All components not listed are zero. T is the uniaxial stress. The corresponding components of the dielectric tensor may be determined by measuring the reflection of light polarized parallel and perpendicular to the stress axis.

[001] stress

$$\delta\epsilon_{2,1}=\delta(\epsilon_{11}+2\epsilon_1)/\sqrt{3},\tag{3.10}$$

$$\delta\epsilon_{2,3\alpha}=(\sqrt{\tfrac{2}{3}})\delta(\epsilon_{11}-\epsilon_1),\tag{3.11}$$

[111] stress

$$\delta\epsilon_{2,1}=\delta(\epsilon_{11}+2\epsilon_1)/\sqrt{3},\tag{3.12}$$

$$\delta\epsilon_{2,5xy}=\delta\epsilon_{2,5xz}=\delta\epsilon_{2,5yz}=\delta(\epsilon_{11}-\epsilon_1)/3.\tag{3.13}$$

The contributions to W come from two sources, strain shifts of energy bands and variation of optical matrix elements with strain. The strain shift contribution is easiest to analyze and satisfies the simplest symmetry relations. For nondegenerate bands the symmetry conditions are given in Table I.

These results have been obtained by group-theoretic methods but most of them are easily explained in an elementary manner. Consider the case of nondegenerate critical points in the [111] direction under a [001] stress. The critical points are clearly all equivalent. (Cubic operations leaving the stress invariant can be found to interchange any pair of critical points.) Thus, their energy shifts must be identical. Identical shifts correspond to the hydrostatic part of the uniaxial stress and contribute only to W_1^{shift}, thus, $W_3^{\text{shift}}=0$.

Since it is generally accepted that the 2.1-eV reflectivity structure comes from critical points in the Λ or L regions, we expect to find $W_3^{\text{shift}}=0$.

The contributions to W from matrix-element variation, which we denote by W^{mvar}, are generally finite for all critical-point locations. For nondegenerate bands, W^{mvar} is inversely proportional to the smallest "direct"-energy separation $E_{n1}(\mathbf{k}_0)$-$E_{n2}(\mathbf{k}_0)$ between bands which are mixed by the strain. Since hydrostatic strain mixes only bands of identical symmetry which are usually well-separated in energy, we expect to find that W_1^{mvar} is very small. In Ge, the L_1-L_1 separation is 8 eV, and the $L_{3'}$-$L_{3'}$ separation is even larger.[7]

The smallest direct-energy separations are usually associated with spin-orbit splittings so that this will usually lead to the largest values of W^{mvar}.

If the 2.1-eV structure in Ge is associated with an L or Λ critical point it undoubtedly corresponds to a transition from an L_{3-} (Λ_3) valence band to an L_{1+} (Λ_1) conduction band. The L_{3-} (Λ_3) orbital degeneracy is removed by spin-orbit interaction giving a Γ_{4-} Kramers doublet and a Γ_{5-}, Γ_{6-} doublet in Koster's notation.[20] These doublets are effectively nondegenerate since they cannot be split by strain.

We can make a quantitative estimate of W^{mvar} within the framework of the effective mass approximation, as discussed in Ref. 15. For kinetic energies or exciton binding energies small compared to the spin-orbit splitting, the kinetic-energy operators of both sets of bands are identical (off-diagonal kinetic-energy terms between spin-orbit split states are neglected). One then obtains a complete spectrum of states $\psi_\pm{}^t$ which may be written

$$\psi_\pm{}^t=\varphi^tU_\pm,\quad\mathcal{E}_\pm{}^t=E^t\pm\lambda+E^0.\tag{3.14}$$

$U_\pm$ is the band-edge pair-band Bloch function with band energy $\pm\lambda+E^0$. The quantity 2λ is the spin-orbit splitting. The function φ^t is an envelope function, and E^t is the energy of state t relative to the band edge. The important point is that φ^t and E^t are independent of whether the state is in band U_+ or U_-. The function φ^t can be taken as a hydrogenic exciton or as an uncorrelated pair in a plane-wave state, $e^{i\mathbf{k}\cdot(\mathbf{r}_1-\mathbf{r}_2)}$. The spectrum of E^t and form of φ^t determines the shape and magnitude of the functions

$$\epsilon_2{}^\pm(\omega)=L(\omega-E^0\mp\lambda),\tag{3.15}$$

but in our model $\epsilon_2{}^+$ and $\epsilon_2{}^-$ are identical except for a translation of the origin.

[20] G. F. Koster, J. O. Dimmock, R. G. Wheeler, and H. Statz, *Properties of the Thirty-Two Point Groups* (The MIT Press, Cambridge, Massachusetts, 1963).

Of course, the unstrained dielectric function ϵ_2^0, is given by

$$\epsilon_2^0(\omega)=\epsilon_2^+(\omega)+\epsilon_2^-(\omega). \tag{3.16}$$

We consider strain effects only within the multiplet of states $\varphi^t U_\pm$. It then follows that one can write:

$$W_1=-\sqrt{3}D_1^1(d/d\omega)\epsilon_2^0(\omega), \tag{3.17}$$

$$W_3=\sqrt{\tfrac{3}{2}}D_3^3(\epsilon_2^+-\epsilon_2^-)/\lambda, \tag{3.18}$$

$$W_5=\sqrt{\tfrac{2}{3}}D_3^5\frac{(\epsilon_2^+-\epsilon_2^-)}{\lambda}+\frac{D_1^5}{2\sqrt{3}}\frac{d}{d\omega}\epsilon_2^0(\omega). \tag{3.19}$$

Using (3.17) and (3.18), Eq. (3.19) can be rewritten

$$W_5=-\frac{1}{6}\frac{D_1^5}{D_1^1}W_1+\frac{2}{3}\frac{D_3^5}{D_3^3}W_3. \tag{3.20}$$

The deformation potentials D_j^i describe the influence of strain on the band edge functions $U_\pm$. In particular, D_1^1 describes the effect of hydrostatic strain which shifts all $\psi_\pm^t(\mathbf{k}_0)$ by the same amount, independent of t, $\pm$, or $\mathbf{k}_0$. Hydrostatic strain thus takes a simple energy derivative of the unperturbed spectrum. This would not be the case if we consider the strain mixing of bands other than $U_\pm$. It would also not be true if D_1^1 varied appreciably over the region of k space contributing to the range of $\epsilon_2(\omega)$ which we study.

D_1^5 represents the effect of strain components which transform like the identity (Γ_1) under the group of $L(\Lambda)$, but transform like Γ_5 under the group of $\mathbf{k}=0$. All states for a given $\mathbf{k}_0=L(\Lambda)$ are shifted by the same amount, but equivalent $\mathbf{k}_0$ shift differently, because the strain tensor has different components when referred to $\mathbf{k}_0'$ rather than $\mathbf{k}_0$.

The deformation potentials D_3^5 and D_3^3 represent strain interactions between U_+ and U_-. They cause the oscillator strength to transfer from band U_+ to U_-. Equation (3.18) follows from (3.14) by first-order perturbation theory as discussed in Ref. 15.

Equations (3.15)–(3.20) are derived on the basis of an effective mass approximation for the pair states together with the more restrictive assumption that the kinetic energy relative to the band edge is small compared to the spin-orbit splitting. We do not assume *anything* about the importance of exciton effects. Such effects influence the shape of the function L in Eq. (3.15) which is determined from experiment.

We do not expect that our assumptions will be accurately obeyed. They provide a convenient basis for analyzing the data and for approximately determining the constants D_j^i.

Some of the relations implied by Eqs. (3.15)–(3.20) will be more accurately obeyed than others. For instance, Eq. (3.17) is valid if hydrostatic band mixing can be ignored, and if D_1^1 does not vary greatly over the region of k space contributing to $\epsilon_2(\omega)$ in the range studied. W_1 and W_3 give two very different line shapes. The first is almost entirely energy-shift effects, and the second almost entirely matrix-element effects. W_5 is seen to be a linear combination of the two. This relation might be more accurate than the effective mass assumptions but it is not easily proven. Experimentally, we find that Eqs. (3.17) and (3.20) are quite accurately obeyed if we adjust the three parameters D_1^1, D_1^5, and D_3^5/D_3^3. Equation (3.18) is less accurate, particularly when the restriction $\epsilon_2^+(\omega+2\lambda)=\epsilon_2^-(\omega)$ is imposed.

Although the analysis presented above in terms of the dielectric constant is certainly the most fundamental approach, it is somewhat inconvenient because of the need for performing a Kramers-Kronig analysis on the measured reflectivity. This procedure may also further compound any errors in the data. It is therefore of interest to see what approximations have to be made in order to perform the analysis on the reflectivity itself without going through the Kramers-Kronig transform. The detailed analysis is presented in the appendix. We summarize the results here.

We define quantities analogous to Eqs. (3.4)

$$\delta\epsilon_{1,j\gamma}=\hat{W}_j e_{j\gamma}, \tag{3.21}$$

where the $\hat{W}_j$ and W_j are related by the Kramers-Kronig relations

$$\hat{W}_j(\omega)=\frac{1}{\pi}P\int_0^\infty W_j(\omega')\left(\frac{1}{\omega'-\omega}+\frac{1}{\omega'+\omega}\right)d\omega'. \tag{3.22}$$

The reflectivity changes may then be written

$$\left(\frac{\delta R}{R}\right)_{j\gamma}=Q_j e_{j\gamma}, \tag{3.23}$$

$$Q_j=\alpha\hat{W}_j+\beta W_j, \tag{3.24}$$

$$\alpha=\frac{2A}{A^2+B^2};\quad \beta=\frac{2B}{A^2+B^2}, \tag{3.25}$$

where A and B are defined in Eq. (3.3). Quantities analogous to the Q_j's have been used by Gerhardt.[21]

Using these definitions, we can then write the analogs of Eqs. (3.17), (3.18), and (3.20) for the Q's

$$Q_1=-\sqrt{3}D_1^1\frac{1}{R^0}\frac{dR^0(\omega)}{d\omega}, \tag{3.26}$$

where R^0 is the unstrained reflectivity

$$Q_3=\sqrt{\tfrac{3}{2}}D_3^3\frac{(R^+-R^-)}{\lambda R}, \tag{3.27}$$

$$\frac{R^\pm}{R}=\alpha\epsilon_1^\pm+\beta\epsilon_2^\pm, \tag{3.28}$$

$$Q_5=-\frac{1}{6}\frac{D_1^5}{D_1^1}Q_1+\frac{2}{3}\frac{D_3^5}{D_3^3}Q_3. \tag{3.29}$$

[21] U. Gerhardt, Phys. Rev. **172**, 651 (1968).

These equations differ in their degree of accuracy. Equation (3.29) is as accurate as (3.20), being a simple consequence of the linearity of all the transformations involved.

Equation (3.26) involves the approximation that we neglect the term

$$\frac{1}{\pi}P\int_0^\infty \frac{W_j(\omega')}{\omega'+\omega}d\omega' \qquad (3.30)$$

on the right-hand side of Eq. (3.22) in comparison to the much larger term with the "resonant" denominator.

Equation (3.27) requires the above approximation, together with the further approximation that the structure in the unstrained reflectivity $R^{\pm}$ is small compared to the reflectivity itself, so that the differential expansion of Eq. (3.28) can be made. This is the least accurate of all the relations but it is still a tolerable approximation at the level of accuracy at which we are able to work.

Using these relations the need for a Kramers-Kronig analysis can be bypassed as far as symmetry analysis and deformation potential constant determination is concerned. Of course, the W_j curves are of more basic significance than the Q_j's so that it is desirable to determine them. The use of the Q's may actually be better for determining deformation potential constants since the errors in the data which get compounded by the Kramers-Kronig analysis may be worse than the approximations we have had to make to justify the reflectivity relations.

A "compromise" version of Eq. (3.27) may also be written, namely,

$$Q_3=\sqrt{\tfrac{3}{2}}\frac{D_3^3}{\lambda}[\alpha(\epsilon_1^+-\epsilon_1^-)+\beta(\epsilon_2^+-\epsilon_2^-)]. \qquad (3.31)$$

This formula obviously requires a Kramers-Kronig analysis of the unstrained reflectivity, but not of the differential reflectivity. It is as accurate as Eq. (3.26), since the approximation involved in (3.28) is not required. The neglect of the expression in (3.30) is still necessary. It may be desirable to use Eq. (3.31) even when (3.28) is not too inaccurate simply because it is more reliable to decompose ϵ_2^0 into $\epsilon_2^{\pm}$ than it is to decompose R^0 into $R^{\pm}$.

IV. DATA ANALYSIS

Figure 2 illustrates the $\delta R/R_{\parallel}$ and $\delta R/R_{\perp}$ data for polarization parallel and perpendicular to the [001] direction, respectively, at 300 and 77°K. It is seen that the structure sharpens as the temperature is lowered to 77°K, and that it moves by 0.09±0.01 eV toward higher energy corresponding to an average temperature coefficient of 4.0×10^{-4} eV/°C. Data were also taken at liquid helium temperatures. The structure at 4°K is essentially the same as that at 77°K except that it is shifted by approximately 0.01 eV toward higher energy.

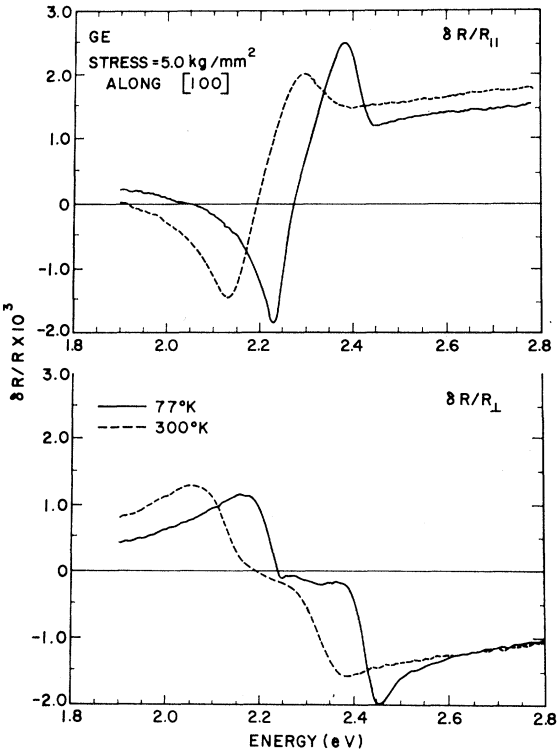

FIG. 2. $\delta R/R$ of Ge for a uniaxial stress of 5.0 kg/mm² along the [001] direction. The dashed and solid curves are for 300 and 77°K, respectively. The upper and lower curves are for the optical electric vector parallel (∥) and perpendicular (⊥) to the stress direction, respectively. The data have been corrected for offset.

Our results for 300°K in the form of the Q_j and W_j are shown in Figs. 3 and 4, respectively. The Q_j defined in Eq. (3.23) are simply the symmetry adapted piezoreflectivities given by the analogs of Eqs. (3.10)–(3.13) divided by the respective symmetry adapted strains defined in Eqs. (3.6)–(3.9). The W_j are obtained through a Kramers-Kronig transformation of the Q_j according to Eqs. (3.1)–(3.2). Potter's[9] 300°K dielectric function data were used to obtain the A and B coefficients in Eq. (3.2).

The two objectives of our data analysis are: (1) To confirm that the structure arises from a critical point in the [111] direction of k space, and (2) to evaluate the four deformation potential constants. We accomplish both of these if we demonstrate that our data are accounted for by the theory in Sec. III. We can work with either the Q_j or W_j. In our case it is advantageous to obtain D_1^1 from Q_1, D_3^3 from W_3, and D_3^5 and D_1^5 from the comparison of Q_5 with Q_1 and Q_3.

Throughout this analysis we use least-squares curve fitting to compare different functions. We define the symbol $\doteq$ to denote that the function to the left-hand side is represented by the functions to the right-hand side in the least squares sense. The fit is obtained by using a digital computer to determine the optimum coefficients C_j.

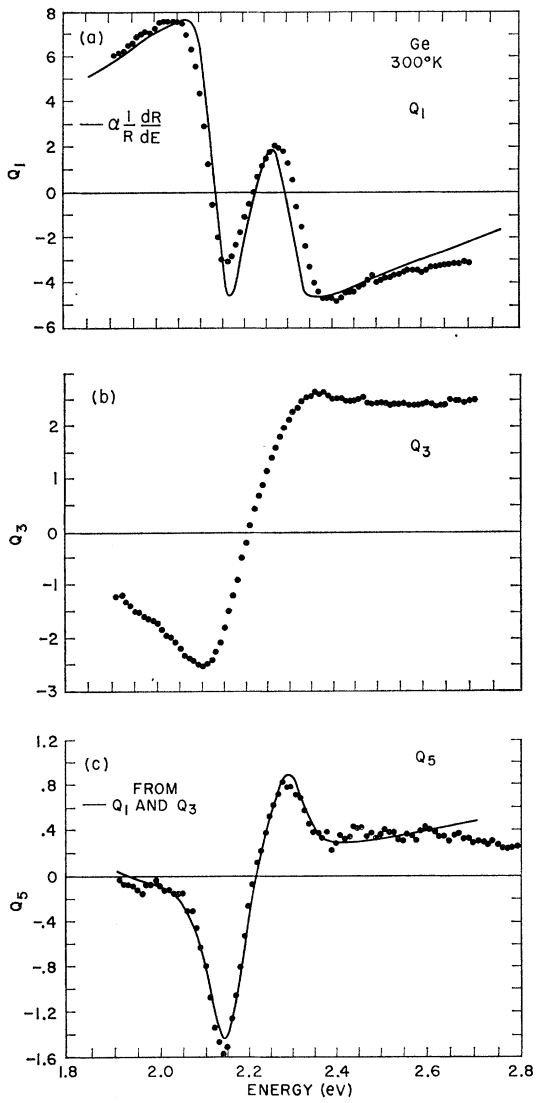

FIG. 3. The Q_1, Q_3, and Q_5 data for Ge at 300°K are plotted as discrete points. The solid curve in (a) is $-\sqrt{3}D_1^1(1/R)(dR/dE)$ with $D_1^1=-9.7$ eV as obtained from Eq. (4.1), using the reflectivity data in Ref. 22. It was necessary to shift the data in Ref. 22 by 0.03 eV to higher energy in order to obtain the correspondence shown here. The solid curve in (c) is the fit obtained from Eq. (4.3), with $D_1^5/D_1^1=-0.77$ and $D_3^5/D_3^3=0.68$.

First let us consider Q_1 shown in Fig. 3(a). We find that the two Q_1's obtained from [001] and [111] oriented crystals are the same (as they should be). Equation (3.26) indicates that Q_1 is proportional to the logarithmic derivative of the unstrained reflectivity. To check this, we calculated $(1/R)dR/dE$ from Gerhardt's[22] 300°K reflectivity data, and then fitted the curve

$$Q_1 \doteq C_1(1/R)dR/dE+C_2, \tag{4.1}$$

with the hydrostatic deformation potential constant given by

$$D_1^1=-C_1/\sqrt{3}. \tag{4.2}$$

[22] U. Gerhardt (to be published).

The solid curve in Fig. 3(a) illustrates the fit obtained for $D_1^1=-9.7\pm1$ eV. The error limits include both the random errors in the data and the uncertainty arising from the data analysis. The fit which is already quite good could probably be improved if both Q_1 and $(1/R)dR/dE$ were obtained from measurements on the same sample.

The constant C_2 in Eq. (4.1) measures the offset in Q_1. The data shown in Fig. 3a have already been corrected by subtracting C_2 from the experimental Q_1.

We cannot use C_2 directly to correct other quantities such as Q_3 and Q_5 because the offset is not completely independent of polarization. Instead we have used the following approach. For some data Q_1 had no appreci-

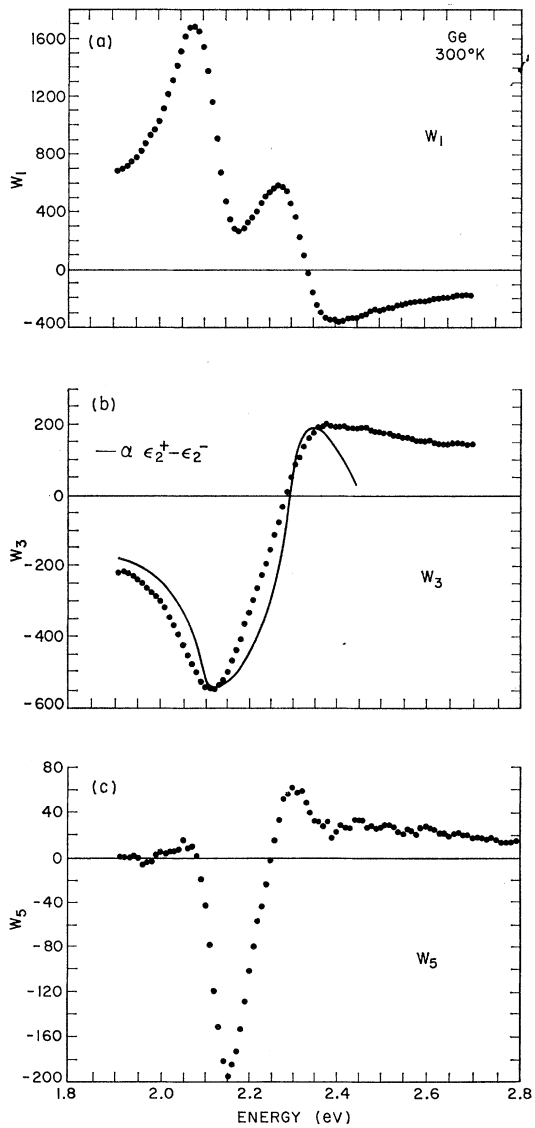

FIG. 4. The W_1, W_3, and W_5 data for Ge at 300°K are plotted as discrete points. The solid curve in (b) is $\sqrt{\frac{3}{2}}(D_3^3/\lambda)(\epsilon_2^+-\epsilon_2^-)$ where $D_3^3=2.2$ eV and $\epsilon_2^\pm$ are obtained from the decomposition of ϵ_2^0.

able offset. We assumed that in this case the offset was zero for both polarizations, and we corrected other experimental runs to have the same zero level as these. In this way we have determined the zero level for all the data in Figs. 2–4.

The presence of offset does not create any great difficulty for our analysis of the Q_j (as long as it is actually energy-independent). It is important though to remove the offset before transforming to the W_j. An offset in Q_j distorts the shape of W_j by contributing a term proportional to $B(\omega)$ to Eq. (3.2).

Next we consider Q_5 shown in Fig. 3(c). Since Eq. (3.29) indicates it should be a linear combination of Q_1 and Q_3, we attempt a fit of the form

$$Q_5 \doteq C_1 Q_1 + C_2 Q_3 + C_3, \tag{4.3}$$

with

$$D_1^5/D_1^1 = -6C_1, \tag{4.4}$$

and

$$D_3^5/D_3^3 = \tfrac{3}{2}C_2. \tag{4.5}$$

Our result for $D_1^5/D_1^1 = -0.77$ and $D_3^5/D_3^3 = 0.68$ is the solid curve in Fig. 3(c). This rather good fit, obtained without the use of any external data, strongly supports the theory and provides rather accurate values for the ratios in Eqs. (4.4) and (4.5). With $D_1^1 = -9.7$, we have $D_1^5 = 7.5 \pm 0.8$ eV. We have assumed that most of the error in D_1^5 arises from the uncertainty in D_1^1.

We note finally that a small value of C_3 in Eq. (4.3) provides a further check that the offset in the data has been removed.

The deformation potential constant D_3^3 is the most difficult one to determine, because we must first determine either $\epsilon_2^{\pm}$ or $R^{\pm}$ which are not directly measurable. Here we choose to work with the more fundamental quantities $\epsilon_2^{\pm}$ and W_3. Equation (3.18) suggests a fit of the form

$$W_3 \doteq C_1(\epsilon_2^{+} - \epsilon_2^{-}) + C_2, \tag{4.6}$$

with

$$D_3^3 = (\sqrt{\tfrac{2}{3}})\lambda C_1. \tag{4.7}$$

To use Eq. (4.6), we must obtain some representation for functions $\epsilon_2^{\pm}$. We have used Potter's data[9] to determine $\epsilon_2^{\pm}(\omega)$ in Eqs. (3.15) and (3.16). We proceed in a purely arbitrary manner by setting $\epsilon_2^{-}(\omega) = C\epsilon_2^{0}(\omega)$ for $\hbar\omega \leq 1.9$ eV. If we select the constant C such that $\epsilon_2^{-}(\omega)$ is continuous at 1.9 eV, Eqs. (3.15) and (3.16) give a unique decomposition of ϵ_2^0 into $\epsilon_2^{\pm}$ as shown in Fig. 5. It appears that our assumption (see Eq. 3.15), that $\epsilon_2^{+}(\omega)$ is equal to $\epsilon_2^{-}(\omega - 2\lambda)$, has lead to the unphysical oscillations in $\epsilon_2^{\pm}$ for energies above 2.4 eV.

The fit obtained from Eq. (4.6) with $D_3^3 = 2.2$ eV is shown as the solid curve in Fig. 4(b). Here we have restricted the least squares fitting to the region near the peaks.

We can obtain another representation of $\epsilon_2^{\pm}$ by using the W_3 data in the relation

$$2\epsilon_2^{\pm} = \epsilon_2^{0} \pm \sqrt{\tfrac{2}{3}}(\lambda W_3/D_3^3). \tag{4.8}$$

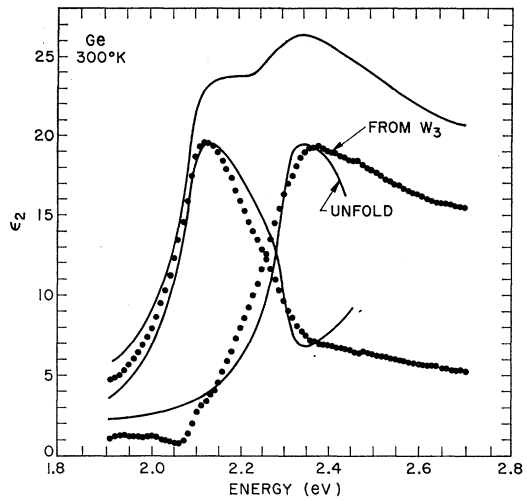

FIG. 5. The upper curve is ϵ_2^0 at 300°K obtained from Ref. 9. The two lower solid curves are $\epsilon_2^{\pm}$ obtained from the decomposition procedure. The two discrete curves are obtained from Eq. (4.8) with $D_3^3 = 2.2$ eV.

The two functions $\epsilon_2^{\pm}$ obtained in this manner, with $D_3^3 = 2.2$ eV, are shown in Fig. 5. It is seen that the functions have different shapes for energies above the peaks. It is not surprising, therefore, that we encountered difficulty in the decomposition of ϵ_2 when we required the shapes of $\epsilon_2^{\pm}$ to be identical.

The experimental reproducibility error in W_3 is less than $\pm 10\%$. We believe, however, that a greater uncertainty in D_3^3 arises from the uncertainty in the $\epsilon_2^{\pm}$. We estimate the error limits to be $D_3^3 = 2.2_{-0.5}^{+1}$ eV.

Even though the ratio D_3^5/D_3^3 should be accurate to $\pm 5\%$, the accuracy of D_3^5 is limited by the uncertainty in D_3^3. From Eq. (4.5), we obtain $D_3^5 = 1.5_{-0.3}^{+0.6}$. More accurate values for D_3^3 and D_3^5 must await a better theoretical understanding of the ϵ_2 line shape.

The values of the deformation potential constants are summarized in Table II. Our value of D_1^1 agrees with the results of Gerhardt[5] and Zallen and Paul,[16] but is somewhat larger than the value obtained by Pollak and Cardona.[6] Gerhardt's[5] value $E_2 = 5.1$ eV is equiv-

TABLE II. Our measurements of the four pair-band deformation-potential constants D_1^1, D_1^5, D_3^3, and D_3^5 compared to other measurements. The values at $k=0$ come from Table III and Eq. (4.9).

	Our measurements (eV)	Other (eV)
D_1^1	-9.7 ± 1	-9.9 ± 0.5[a,b]
		-7.8 ± 0.7[c]
D_1^5	7.5 ± 0.8	5.9 ± 1.2[b]
D_3^3	$2.2_{-0.5}^{+1}$	2.6 $k=0$[c]
D_3^5	$1.5_{-0.3}^{+0.6}$	6.4 $k=0$[c]
2λ	0.21	0.20 $k=0$[c]
D_1^5/D_1^1	-0.77 ± 0.04	
D_3^5/D_3^3	0.68 ± 0.03	0.43[d] $k=L$

[a] Reference 16. [b] Reference 5. [c] Reference 6. [d] Reference 14.

TABLE III. Relations between the single-band deformation potential constants, d_j^i, at L and at Γ assuming that the periodic parts of the wave function do not change. The relation between our notation and that of Kleiner and Roth (Ref. 24) or Pikus and Bir (Ref. 25) is also given. The numerical values originate from Ref. 26. The pair-band deformation potential constants are obtained from Eq. (4.9).

Our notation	Kleiner and Roth	Pikus and Bir	Measured in eV
$d_1^1(L)\approx d_1(\Gamma)$	$=\sqrt{3}D_d^v$	$=\sqrt{3}a$	
$d_1^5(L)\approx\frac{-d_5}{\sqrt{2}}(\Gamma)$	$=\frac{2}{\sqrt{3}}D_{u'}$	$=-d$	$=4.5$
$d_3^3(L)\approx\frac{d_3(\Gamma)}{\sqrt{2}}$	$=-\sqrt{\frac{2}{3}}D_u$	$=\sqrt{\frac{3}{2}}b$	$=-2.6$
$d_3^5(L)\approx d_5(\Gamma)$	$=-\frac{2\sqrt{2}}{\sqrt{3}}D_{u'}$	$=\sqrt{2}d$	$=-6.4$
$l(L)\approx-\frac{1}{3}\Delta(\Gamma)$	=		$=-0.10$

alent to $D_1^5=(2/\sqrt{3})E_2=5.9\pm1.2$ eV in our notation. Our more accurate value is consistent, within errors, with his result. The quantities D_3^3 and D_3^5 have not been measured previously although they were implicitly determined to be equal to the values at $k=0$ by Pollak and Cardona.[6]

It is seen that analysis of piezoreflectivity requires rather accurate reflectance and/or dielectric function data. Such data are not available for an analysis of our 77°K results. We have, however, used Potter's 120°K data to analyze W_1 and W_3. On the other hand, we can use our own data to decompose Q_5 according to Eq. (4.3). The resulting deformation potential constants are consistent with the values in Table II but are probably somewhat less accurate.

It is very easy to relate the pair-band deformation and spin-orbit parameters to the single-band parameters since the conduction band has L_1 (Λ_1) symmetry. The relations are

$$D_j^i=d_1^{ci}\delta_{j1}-d_j^{vi} \tag{4.9}$$

and

$$\lambda=-l^v,$$

where the superscripts v and c refer to the valence and conduction single band parameters. Here l is $\frac{1}{2}$ the single band spin-orbit splitting. δ_{j1} is Kronecker's δ.

If the critical point is the L point, the parameter d_1^{c5} is known from a variety of measurements. In Herring's notation[23]

$$d_1^{c5}=\Xi_u/\sqrt{3}\approx10\text{ eV}. \tag{4.10}$$

Pollak and Cardona[6] have suggested on the basis of $\mathbf{k}\cdot\mathbf{p}$ calculations that the two upper valence band wave functions in the Λ direction are nearly the same as at $k=0$. One can then estimate the parameters d^v and l^v from the measured values at $k=0$. See also Refs. 24–26.

The appropriate relations are given in Table III. With these values, we can make a comparison to our measured values as shown in Table II.

V. DISCUSSION AND SUMMARY

The line shapes for the three fundamental response functions W_1, W_3, and W_5 are given in Fig. 4, and their reflectivity analog Q_j are given in Fig. 3. Together, they constitute the principal results of this paper. We have given a detailed quantitative description of the interpretation of these line shapes which constitute a very convincing proof that the critical points at 2.1 and 2.3 eV lie in the Λ direction or at the L point. A number of independent results have strongly suggested this conclusion previously. The approach most closely related to our own is the dc strain dependence of the polarized reflectivity measured by Gerhardt.[5] Our work is more detailed and, we feel, even more convincing. More importantly, our approach is directly applicable to other materials whose band structures are more controversial than Ge and should be more generally useful than the dc strain techniques since many materials cannot sustain the high strains required by the dc method.

The line shapes W_1 and W_3 or Q_1 and Q_3 are very distinctive. W_1 or Q_1 represent the hydrostatic response and are very nearly the derivative of the unstressed response as shown for Q_1 in Fig. 3. W_3 or Q_3 represent purely matrix element changes because of the critical point symmetry. The line shape reflects a transfer of oscillator strength from one spin-orbit split band to the other. W_5 or Q_5 contain terms which lead to both energy shifts and matrix element changes and in Fig. 3(c) we see that Q_5 can be reasonably well represented as a linear superposition of Q_1 and Q_3.

The amplitudes of the W functions are controlled by four deformation potential parameters; D_1^1, D_1^5, D_3^3, and D_3^5 in our notation. The relation of this notation to other more standard notations is given in Table III and the values we have obtained for these quantities are given in Table II.

The procedure for determining the D's has been discussed in Sec. IV. The values for D_3^3 and D_3^5 in Table II are compared to their analogs at $k=0$. Pollak and Cardona[6] have analyzed their piezoelectroreflectance results at 2.2 eV in terms of the $k=0$ values and find good agreement. As seen in Table II, all our values are in reasonable agreement with measurements obtained by other methods, except D_3^5. The discrepancy here is a factor of 4 and is well outside our limits of error. We have not considered valley-orbit interactions or electron-hole spin-spin coupling due to exchange in our analysis. It seems unlikely that these effects could

[23] C. Herring and E. Vogt, Phys. Rev. **101**, 944 (1956).
[24] W. H. Kleiner and L. M. Roth, Phys. Rev. Letters **2**, 334 (1959).
[25] G. E. Pikus and G. L. Bir, Fiz. Tverd. Tela **1**, 1642 (1959) [English transl.: Soviet Physics—Solid State **1**, 1502 (1959)].
[26] J. C. Hensel, Phys. Rev. Letters **21**, 983 (1968) contains $D_{u'}=+3.9$ eV. We also have $D_u=+3.2$ eV. J. C. Hensel (private communication).

account for a factor of 4. Uncertainties in D_3^3 contribute to the uncertainty in D_3^5 because the Q_5 analysis determines D_3^5/D_3^3. These uncertainties can be bypassed by comparing the ratios directly. The ratios still differ by a factor of 3.6 which focuses the discrepancy entirely onto the assumption that Q_5 can be uniquely represented as a linear combination of Q_1 and Q_3. The agreement in Fig. 3 is really quite good and the line shapes of Q_1 and Q_3 are sufficiently distinct that very little parameter variation is possible. We must conclude that the disagreement is genuine.

We have used the recent theoretical calculations of Saravia and Brust[14] to deduce a value of D_3^5/D_3^3 at the L point. We find $D_3^5/D_3^3=(\alpha_{111}/\alpha_{100})^{1/2}=0.43$. The value of 0.68, which we have measured, lies between the values at L and Γ, which tends to support our value.

ACKNOWLEDGMENTS

The authors are indebted to A. U. MacRae who made his preliminary results on Ge available to us. We are also grateful to G. D. Stohlbom for much experimental assistance, to A. J. Williams for constructing the original stress-modulation apparatus, and to Miss B. Cetlin for computer programming assistance.

APPENDIX

We here derive the results presented in Sec. III which show that one can avoid the Kramers-Kronig analysis in studying the differential reflectivity at the cost of only a small error.

We take the $\delta\epsilon_1$ analog of Eq. (3.2) from Garfinkel, Tiemann, and Engeler[2] and write

$$\delta\epsilon_1=A\tfrac{1}{2}(\delta R/R)+B\delta\theta, \tag{A1}$$

where A and B are defined in Eq. (3.3). Equations (3.2) and (A1) can then be solved for $\delta R/R$

$$\delta R/R=\alpha\delta\epsilon_1+\beta\delta\epsilon_2, \tag{A2}$$

$$\alpha=2A/A^2+B^2;\quad \beta=2B/A^2+B^2. \tag{A3}$$

The Kramers-Kronig relations between $\delta\epsilon_1$ and $\delta\epsilon_2$ may be written

$$\delta\epsilon_1(\omega)=\frac{1}{\pi}P\int_0^\infty \delta\epsilon_2(\omega')\left(\frac{1}{\omega'-\omega}+\frac{1}{\omega'+\omega}\right)d\omega', \tag{A4}$$

where P denotes the principal value.

If we substitute Eqs. (3.4) into (A4) the linearity allows us to write

$$\delta\epsilon_{1,j\gamma}=\hat{W}_j e_{j\gamma}, \tag{A5}$$

$$\hat{W}_j(\omega)=\frac{1}{\pi}P\int_0^\infty W_j(\omega')\left(\frac{1}{\omega'-\omega}+\frac{1}{\omega'+\omega}\right)d\omega'; \tag{A6}$$

and Eq. (A2) leads to

$$(\delta R/R)_{j\gamma}=Q_j e_{j\gamma}, \tag{A7}$$

$$Q_j=\alpha\hat{W}_j+\beta W_j. \tag{A8}$$

Quantities analogous to Q_j have been used by Gerhardt.[21]

It is easy to see, again by linearity, that Eq. (3.20) holds if $\hat{W}_j$ or Q_j is substituted for W_j, namely,

$$Q_5=-\frac{1}{6}\frac{D_1^5}{D_1^1}Q_1+\frac{2}{3}\frac{D_3^5}{D_3^3}Q_3. \tag{A9}$$

We now make the approximation of neglecting the second term in the integrand in Eq. (A4) in comparison to the first. This term is smaller because it is "nonresonant" and much less rapidly varying with ω, so this should be quite a good approximation for analyzing any sort of sharp structure. This approximation will be used throughout the remainder of the appendix. Using the well-known relation

$$1/x+i\epsilon=P/x-i\pi\delta(x),$$

we transform our approximate version of (A4) to

$$\delta\epsilon_1(\omega)=\frac{1}{\pi}\int_0^\infty\frac{\delta\epsilon_2(\omega')d\omega'}{(\omega'-\omega+i\epsilon)}+i\delta\epsilon_2(\omega). \tag{A10}$$

This form is useful when we integrate by parts.

We now attempt to extend Eq. (3.17) to its Q_1 analog. Substituting (3.17) into (A10) gives:

$$\hat{W}_1(\omega)=-\sqrt{3}D_1^1\left(\frac{1}{\pi}\int_0^\infty\frac{d}{d\omega'}\epsilon_2^0(\omega')\frac{1}{\omega'-\omega+i\epsilon}d\omega'+i\frac{d}{d\omega}\epsilon_2^0(\omega)\right). \tag{A11}$$

Then an integration by parts and the use of the identity

$$\frac{d}{d\omega'}\frac{1}{(\omega'-\omega)}=-\frac{d}{d\omega}\frac{1}{(\omega'-\omega)} \tag{A12}$$

allows us to write (A11) as

$$\hat{W}_1(\omega)=-\sqrt{3}D_1^1\left(\frac{1}{\pi}\frac{d}{d\omega}\int_0^\infty\frac{\epsilon_2^0(\omega')}{(\omega'-\omega+i\epsilon)}+i\frac{d}{d\omega}\epsilon_2^0(\omega)\right). \tag{A13}$$

Equation (A10) then permits us to write

$$\hat{W}_1(\omega)=-\sqrt{3}D_1^1\,d\epsilon_1^0(\omega)/d\omega. \tag{A14}$$

We now substitute Eqs. (3.17) and (A14) into (A8), and use (A2) to obtain

$$Q_1=-\sqrt{3}D_1^1 dR^0(\omega)/d\omega R^0, \tag{A15}$$

where R^0 is the unstrained reflectivity. ($R^0=R$, the superscript is added for emphasis).

Finally, we wish to study the relations for $\hat{W}_3$ and Q_3 which are the analogs of Eq. (3.18).

We substitute Eq. (3.15) into (A10), and derive the relation

$$\epsilon_1^{\pm}(\omega)=\hat{L}(\omega-E^0\mp\lambda)$$

$$\hat{L}(\omega-E^0)=\frac{1}{\pi}P\int_1^{\infty}\frac{L(\omega'-E^0)}{\omega'-\omega}d\omega'. \quad \text{(A16)}$$

Thus, we have

$$\hat{W}_3=\sqrt{\tfrac{3}{2}}D_3^3(\epsilon_1^+-\epsilon_1^-)/\lambda \quad \text{(A17)}$$

in exact analogy to Eq. (3.18) for W_3.

However, we cannot now proceed to the analogous relation for Q_3 without making a further approximation. We must assume that the structure in the reflectivity is small compared to the reflectivity itself, so that we can use Eq. (A2) to write

$$R^{\pm}/R=\alpha\epsilon_1^{\pm}+\beta\epsilon_2^{\pm}. \quad \text{(A18)}$$

Equation (A18) then allows us to write

$$Q_3=\sqrt{\tfrac{3}{2}}D_3^3(R^+-R^-)/\lambda R. \quad \text{(A19)}$$

The accuracy of (A18) can be tested using results from Kramers-Kronig analyses on the unstrained reflectivity.

Our principal results are Eqs. (A7), (A9), (A15), and (A19) which are in exact analogy to Eqs. (3.4), (3.20), (3.17), and (3.18) for the W_j's. Note that (A7) and (A9) for the Q's are as accurate as the corresponding equations for the W's. Equation (A15) requires an approximation which should generally be quite good. Equation (A19) requires a further approximation which is less accurate but can be checked if ϵ_1 and ϵ_2 are known for the unstrained crystal. Alternatively, one can use the relationship

$$Q_3=\sqrt{\tfrac{3}{2}}(D_3^3/\lambda)[\alpha(\epsilon_1^+-\epsilon_1^-)+\beta(\epsilon_2^+-\epsilon_2^-)]. \quad \text{(A20)}$$

Equation (A20) is much more accurate than (A19), and should compare to (A15) in accuracy. The only approximation required to derive (A20) from (3.18) was the neglect of the nonresonant denominator in Eq. (A4) as in Eq. (A10). If $\epsilon_2^{\pm}$ has been determined, Eqs. (A16) specify $\epsilon_1^{\pm}$.

PHYSICAL REVIEW VOLUME 185, NUMBER 3 15 SEPTEMBER 1969

Observation of Mixed-Mode Excitons in the Photoluminescence of Zinc Oxide

R. L. WEIHER AND W. C. TAIT
3M Company, Central Research Laboratories, St. Paul, Minnesota 55101
(Received 26 March 1969)

Mixed-mode excitons have been previously reported in the absorption spectrum of uniaxial II-VI crystals when plane-polarized light is used with its **E** field in a plane containing both the photon's wave vector **k** and the c axis of the crystal. Lines due to annihilation of mixed-mode excitons should also be observed in the emission spectrum of these uniaxial crystals. We describe here the observation of such emission lines in the photoluminescence of ZnO at 77°K. The strengths of these lines are essentially zero when $\mathbf{k}\perp c$, but increase rapidly as the angle between **k** and c is reduced below 90°. The energies of the A and B longitudinal excitons in Thomas's line assignment are found to be 3.373 and 3.386 eV, respectively, in good agreement with results obtained from reflectivity data.

IT has been shown theoretically by Hopfield and Thomas[1] that "longitudinal" excitons should be optically observable in uniaxial crystals. In that same paper, they demonstrated the existence of longitudinal excitons in ZnO by optical-absorption measurements. Similar observations have been made on CdS by Hopfield and Thomas[2] and on CdSe by Parsons, Wardzynski, and Yoffe[3] and by Wheeler and Dimmock,[4] as well as by other investigators.

The actual absorption lines observed are due to "mixed-mode" excitons which have components of both transverse and longitudinal polarizations. As shown by Hopfield and Thomas,[1] mixed-mode excitons are observed only when the light is polarized with the electric field (**E**) in a plane containing both the photon propagation vector (**k**) and the c axis with the **k** vector at some internal angle ϕ, after refraction, with the c axis as shown in Fig. 1. When the angle ϕ is 0° ($\mathbf{k}\|c$), the excitons are pure transverse, and when $\phi=90°$ ($\mathbf{k}\perp c$), they are pure longitudinal. At all other angles, mixed-mode excitons are observed.

Two notable features of the mixed-mode excitons are the dependences of their oscillator strength and their position in energy on the angle ϕ. The oscillator strength of the mixed mode is given by[1]

$$4\pi\beta_{mx}=4\pi\beta_T\cos^2\phi, \quad (1)$$

where $4\pi\beta_T$ is the oscillator strength of the transverse mode. The position, in energy, of the mixed mode is[1]

$$E_{mx}=E_T[1+(4\pi\beta_T/\epsilon)\sin^2\phi]^{1/2}, \quad (2)$$

where E_T is the energy of the transverse mode and ϵ is the dielectric constant due to all higher energy transitions.

[1] J. J. Hopfield and D. G. Thomas, J. Phys. Chem. Solids **12**, 276 (1960).
[2] J. J. Hopfield and D. G. Thomas, Phys. Rev. **122**, 35 (1961).
[3] R. B. Parsons, W. Wardzynski, and A. D. Yoffe, Proc. Roy. Soc. (London) **A262**, 120 (1961).
[4] R. G. Wheeler and J. O. Dimmock, Phys. Rev. **125**, 1805 (1962).